Electronic structure of thin films by the self-consistent numerical-basis-set linear combination of atomic orbitals method: Ni(001)

C. S. Wang

Department of Physics and Astronomy and Materials Research Center, Northwestern University, Evanston, Illinois 60201

A. J. Freeman

*Department of Physics and Astronomy and Materials Research Center, Northwestern University, Evanston, Illinois 60201
and Argonne National Laboratory, Argonne, Illinois 60439*
(Received 8 June 1978)

We present the self-consistent numerical-basis-set linear combination of atomic orbitals (LCAO) discrete variational method for treating the electronic structure of thin films. As in the case of bulk solids, this method provides for thin films accurate solutions of the one-particle local density equations with a non-muffin-tin potential. Hamiltonian and overlap matrix elements are evaluated accurately by means of a three-dimensional numerical Diophantine integration scheme. Application of this method is made to the self-consistent solution of one-, three-, and five-layer Ni(001) unsupported films. The LCAO Bloch basis set consists of valence orbitals ($3d$, $4s$, and $4p$ states for transition metals) orthogonalized to the frozen-core wave functions. The self-consistent potential is obtained iteratively within the superposition of overlapping spherical atomic charge density model with the atomic configurations treated as adjustable parameters. Thus the crystal Coulomb potential is constructed as a superposition of overlapping spherically symmetric atomic potentials and, correspondingly, the local density Kohn-Sham ($\alpha = 2/3$) potential is determined from a superposition of atomic charge densities. At each iteration in the self-consistency procedure, the crystal charge density is evaluated using a sampling of 15 independent k points in (1/8)th of the irreducible two-dimensional Brillouin zone. The total density of states (DOS) and projected local DOS (by layer plane) are calculated using an analytic linear energy triangle method (presented as an Appendix) generalized from the tetrahedron scheme for bulk systems. Distinct differences are obtained between the surface and central plane local DOS. The central plane DOS is found to converge rapidly to the DOS of bulk paramagnetic Ni obtained by Wang and Callaway. Unlike the result of earlier non-self-consistent calculations, only a very small surplus charge (0.03 electron/atom) is found on the surface planes—in agreement with jellium model calculations.

I. INTRODUCTION

Transition-metal surfaces have become a subject of intense interest and study.[1-14] As in the case of bulk transition-metal studies, which have taken place over the last 40 years, the difficulty of treating localized d electrons along with the itinerant s-p electrons has provided the challenge and impetus for developing the sophisticated theoretical methods necessary for accurately determining the electronic structure of transition-metal surfaces. For bulk systems, considerable progress has been made in the last few years in this direction.[15,16] Band-structure calculations of the electronic properties of transition-metal surfaces within the thin-film model include multiple scattering,[1-4] tight binding,[5-8] and supplemented orthogonalized plane-wave methods.[9,10] Kasowski[2] applied the linear combination of muffin-tin orbitals technique to study the energy bands and surface states of a 20-layer Ni (001) film at high-symmetry points in the two-dimensional Brillouin zone (BZ). In a parametrized linear combination of atomic orbitals (LCAO) spin-polarized calculation for a 35-layer Ni (001) film, Dempsey and Kleinman[8] showed that the existence of surface

states above the majority-spin band throughout the two-dimensional BZ could account for the reversal of photoelectron spin polarization observed 0.1 eV above threshold.[17] While providing valuable information about surface properties, these calculations are restricted by the arbitrariness in choosing a non-self-consistent (SC) potential, tight binding, or other parameters. In a recent study of the effects of different non-SC potentials on surface states in Fe, Caruthers and Kleinman[10] concluded that SC is important for transition-metal film calculations in that both the existence and the symmetry of some surface states depend crucially on the details of the potential.

The first self-consistent calculation for a transition-metal surface was made for Nb(100) using a pseudopotential scheme.[11] Due to the localized nature of the d electrons, approximately 1000 plane waves ranging over an energy of 10.2 Ry were required to form the basis set.[18] Convergence tests for bulk Nb[12] indicated that the s, p levels and the d-band width were converged to 0.01 eV, and that the d level may shift relative to s-p levels by as much as 0.2 eV when additional plane waves up to an energy of 16 Ry were included by a perturbation technique. While the *ab initio* SC lin-

ear combination of atomic Gaussian orbitals (LCGO) calculations for Cu(100) and Ni(100) required a much smaller basis set,[13,14] the variational flexibility of their basis set may be limited by the neglect of the atomic $4p$ states. [Note that the state of purely $4p$ symmetry (L_2') is occupied in both bulk Cu and the bulk majority-spin-state Ni bands. In addition, the pure $4p$ state X_4, which influences the slope of the Δ_1 bands arising from the d-band complex, and therefore the position of the Fermi energy relative to the top of the d band in bulk Cu, is missing.] Both the pseudopotential and LCGO methods achieved self-consistency using the symmetrized-plane-wave (SPW) expansion of the charge density. However, due to the lack of periodicity along the surface normal direction, this procedure is very cumbersome for the following reasons. First, although it is possible to artificially restore the periodicity at a long distance away from the surface, the z component of the reciprocal-lattice vectors (K_z) is so small that an enormous number of SPW must be included to obtain a fairly smooth density. Second, the large Fourier coefficients at very small K_z, which vanish in the bulk systems (as required by the periodic boundary conditions), tend to slow down the convergence rate in the surface calculation. Third, the relatively long-range behavior of the surface dipole moment may require additional spacing between two adjacent surface layers in a SC calculation in order to keep them from interacting with each other. For these reasons it is extremely difficult in the plane-wave expansion method to reproduce the sharp structure near the nuclear sites accompanying the charge transfer away from the surfaces.

The degree of self-consistency obtained is determined by the accuracy of the crystal charge density in the calculations. However, due to the complexity of the problem, both of the existing SC calculations[11,13,14] were limited, in sampling the crystal charge density in the SC cycle, to the use of only three special k points in $\frac{1}{8}$ of the independent two-dimensional BZ. The special-k-points formalism is based on the premise that the integrand is relatively smooth in k space, so that it results in a rapidly convergent Fourier expansion. While it has been applied successfully to semiconductors, the convergence of the results obtained with increasing number of sampling k points for a complex d-band charge density in a metal with a sharp step function at the Fermi energy needs to be more carefully explored. In particular, the problem could be quite serious in the case of Ni, where the Fermi energy crosses the upper d-band complex.[19] The self-consistent potential is more sensitive to the concentration of the localized

d electrons in the transition metals than it is to the free-electronlike s-p states. Yet, the d holes on each layer of a Ni film can only be determined accurately after the effects of the cutoff of the Fermi energy are properly included.

Bearing this in mind, we propose in this paper a simpler procedure to account for the major features in SC calculations. The SC numerical-basis-set (LCAO) method of Ellis and Painter[20] and Zunger and Freeman[21] for bulk systems was generalized for the case of an unsupported thin film. A detailed description of the method as applied to one-, three-, and five-layer Ni films is presented in Sec. II. Systematic changes as the film thickness increases are discussed when the band structure and density of states one, three, and five layers of Ni (001) film are compared in Sec. III. Results obtained are compared with experiments and with other theoretical studies. In Sec. IV the effect of SC is discussed. Finally, a two-dimensional BZ integration method to calculate density of states, Fermi energy, and charge density, which was generalized from the linear-analytic-tetrahedron scheme of Jepson and Anderson[22] and Lehmann and Taut[23] for bulk systems,[24] is given in Appendix A; convergence tests and results for a Ni (001) monolayer are given in Appendix B.

II. METHOD

We consider a film of m layers with the origin of the system midway between the two surface layers and the z axis normal to the surfaces. The unit cell consists of a parallelepiped whose z dimension extends to $\pm\infty$. The Coulomb potential is formed as a non-muffin-tin superposition of spherical atomic potentials that can contain long-range ionic components to account for charge transfer in the film. A superposition of overlapping spherical atomic charge densities is used to construct the local density Kohn-Sham ($\alpha = \frac{2}{3}$) $\rho^{1/3}$ exchange potential.[25] Atoms up to 25 a.u. away from the atomic site were included in the two-dimensional direct-lattice sum to obtain the superposition potential and charge density. The long-range ionic component of the Coulomb potential accompanying the charge transfer near the surface is included through a generalized Ewald-type procedure.[26]

To reduce the dimension of the secular equation, the numerical LCAO Bloch basis functions are orthogonalized to the (frozen) atomic core states.[27] The energy of the core states in the atoms at the surface layers are shifted with respect to that of the center plane due to the reduction in the number of nearest neighbors and surface dipole moments. Their overall energy dispersion in k space, however, remains quite small, so that the Bloch core

states can still be approximated by the atomic wave functions to good accuracy. We have used as basis set numerical atomic $3d$, $4s$, and $4p$ orbitals for each Ni atom, generated from a Herman-Skillman-type atomic program,[28] but with the long-range tails of the virtual states suppressed by an additional potential well to avoid the possible occurrence of linear dependencies in the basis set.

Having tabulated the initial potential and Bloch basis functions, the Hamiltonian and overlap matrices that appear in the usual linear variational secular equation are calculated directly by a numerical three-dimensional Diophantine integration scheme[29] without decomposition into multicenter integrals. The unit cell in the form of an infinitely long parallelepiped is divided into three regions, defined in Fig. 1. Within region I, the Diophantine points inside spheres of radius R centered at each atomic site μ are generated in spherical coordinates. Most of the difficulty in the numerical integration comes from treating the Coulomb singularity near the site of the nuclei where the potential is nearly spherically symmetric and the wave functions are of predominantly s-like character. For a spherically symmetric integrand, a three-dimensional numerical integral is equivalent to a one-dimensional radial integral having the same number of Diophantine points. Furthermore, the corresponding weighting factor, which is proportional to the square of the distance from the nucleus, tends to smooth out the integrand near the nucleus, and provides a rather rapid convergence rate. No sampling points are required in the vacuum region II ($|z|>L$), where the charge density vanishes. Finally, the sampling points in the interstitial region III are generated in Cartesian coordinates with equal weights. The method is a very simple and straightforward one to use, regardless of the complexity of the system considered. In the case of a transition metal the rate of convergence of the numerical integrals in the Hamiltonian matrices is determined by the necessity of sampling sharp spikes in the core wave functions with the Coulomb singularity near the nuclear sites. These problems are avoided in using the frozen core approximation. As an illustration of convergence of the results with respect to the number of Diophantine points used in the different regions, we present some results for a monolayer of Ni(001) in Appendix B.
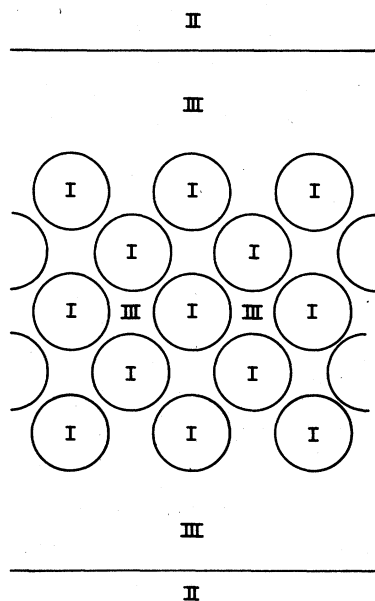
After solving the secular equation, the crystal charge density is computed by integrating the square of the wave functions $|\psi|^2$ over the occupied portion of the two-dimensional BZ. In order to accurately account for detailed Fermi-surface effects, we developed the analytic-linear-energy-triangle scheme as a generalization of the analytic-linear-energy-tetrahedron method[22-24] for bulk systems, using energies and wave functions at 15 equally spaced points in $\frac{1}{8}$ of the irreducible zone. A detailed description of the method as applied to the computation of the density of states, Fermi energy, and charge density is given in Appendix A. This procedure has the advantage over the special-$\vec{k}$-points method in that the contribution from the occupied portion of a triangle can be evaluated exactly as a linear combination of subdivided triangles if we assume that the energy and $|\psi|^2$ vary linearly inside each triangle.

The self-consistent potential within the superposition model is obtained iteratively by varying the atomic configuration as an adjustable parameter. In some of our early calculations, we used the Mulliken[30] charge and population analysis. The Mulliken analysis amounts to arbitrarily dividing equally, between the relevant sites, all the cross terms in the charge-density expression between basis functions located on different inequivalent sites. However, due to the extensive overlap with the $4p$ states from different atomic sites, the converged results overestimate the $4p$ concentration. For this reason, we have developed, instead, a least-mean-squares fitting procedure under the constraint of charge neutrality and the Pauli exclusion principle at selected points in $\vec{r}$ space. The Diophantine points, which have higher density inside region I than in region III, are selected on an equally spaced grid. In addition, we have added

FIG. 1. Schematic representation of the regions over which the Diophantine integration scheme is carried out using the sampling integration points assigned in the text.

TABLE I. Integration parameters, input atomic configuration for the SC potential, and the degree of SC (Δ) for the one-, three-, and five-layer Ni (001) films. (See text or definition of R and L.)

No. of layers	1	3	5
N_I	750	750	600
N_{III}	1500	2000	3000
R (a.u.)	2.2	2.2	2.2
L (a.u.)	8.324 25	11.653 95	14.983 65
SC configuration			
First (center)	$3d^{8.68}4s^{1.20}4p^{0.12}$	$3d^{8.47}4s^{1.43}4p^{0.42}$	$3d^{8.42}4s^{1.30}4p^{0.22}$
Second		$3d^{8.51}4s^{1.25}4p^{0.08}$	$3d^{8.48}4s^{1.51}4p^{0.11}$
Third			$3d^{8.54}4s^{1.35}4p^{0.04}$
Δ	0.187	0.249	0.361
Valence electrons per unit cell	10	30	50
E_F (eV)	−5.61	−5.38	−5.52

points very close to the nuclei in order to ensure that the cusp behavior at a nuclear site is fitted correctly. After taking account of the reflection symmetry about the center plane, we find that around 250–600 points are usually enough to fit three, six, or nine valence-state configurations in the one-, three-, or five-layer Ni (001) films, respectively.

At each iteration, the degree of self-consistency is examined by calculating

$$\Delta = \left[\int_{unit\ cell} (\rho_{crys}^{(\vec{r})} - \rho_{sup}^{(\vec{r})})^2 d^3r \right]^{1/2} , \qquad (1)$$

where ρ_{crys} and ρ_{sup} are the crystal and superposition charge density, respectively. Since Hamiltonian and overlap matrix elements are computed by three-dimensional numerical integration techniques, there is some accumulation of numerical errors in ρ_{cry} . In Appendix B, we discuss the convergence of the wave functions by examining Δ and the Mulliken charge analysis of the wave functions using different sets of Diophantine points. This shows that Δ should be viewed in the superposition model as an upper bound to the difference $\delta\rho$ between ρ_{sup} and the true ρ_{cry}.

At each iteration, the fitting coefficients are compared with those results of the Mulliken charge and population analysis of the wave functions and the input atomic configuration, and are modified accordingly in the next iteration to generate a new superposition potential and overlapping charge density. The final SC configuration is determined by the minimum of Δ. This method has been applied successfully to a Cu (001) monolayer,[31] the

one-, three-, and five-layer paramagnetic Ni (001) films discussed here, and an ordered overlayer of $c(2 \times 2)$ oxygen chemisorbed on the surfaces of a three-layer Ni (001) film[32] using sampling points comparable to those of column E in Tables III and IV. Usually around 5–12 iterations are required to reduce Δ by 40%–60% from its starting value at the zeroth iteration. The resulting Δ, which is an upper bound of the true differences, ranged from 1.87% to 0.72% of the total number of valence electrons in the unit cell.

In principle, it is possible to further minimize Δ by expanding $\delta\rho$ in a more complete set of functions such as symmetrized plane waves or Gaus-

TABLE II. Layer-by-layer projection of the valence-state charge density as calculated by nearest volume integration of ρ_{cry} (cf. column A) and ρ_{sup} (cf. column B). The input atomic configuration and the corresponding Mulliken analysis are given in columns (C) and (D), respectively.

(a) Non-SC potential layer	A	B	C	D
First (center)	10.89	10.00	10.00	10.86
Second	10.73	9.97	10.00	10.97
Third (surface)	8.82	10.03	10.00	8.60
(b) SC potential layer	A	B	C	D
First (center)	10.01	9.98	9.94	9.95
Second	9.96	10.01	10.10	10.15
Third (surface)	10.03	10.00	9.93	9.88

TABLE III. Comparison of the energy-band eigenvalues at high-symmetry points for a Ni (001) monolayer calculated for a superposition model potential $(3d^9 4s^1)$ with different sets of Diophantine points in regions I and III (cf. Fig. 1) for both frozen-core and full basis functions. Units are eV; the zero of energy is the vacuum.

Core	A Full	B Full	C Full	D Frozen	E Frozen	F Frozen
N_I	300	750	1000	1000	750	300
N_{III}	600	1500	2500	2500	1500	600
Γ_1	-9.22	-9.20	-9.22	-9.29	-9.27	-9.31
Γ_3	-6.07	-6.18	-6.20	-6.21	-6.20	-6.20
Γ_1	-4.92	-5.13	-5.14	-5.15	-5.15	-5.24
Γ_5	-3.88	-3.90	-3.91	-3.92	-3.92	-3.93
Γ_4	-3.34	-3.56	-3.58	-3.58	-3.59	-3.58
X_1	-6.19	-6.23	-6.26	-6.27	-6.26	-6.25
X_3	-5.57	-5.59	-5.60	-5.61	-5.60	-5.62
X_2	-4.19	-4.40	-4.41	-4.43	-4.42	-4.48
X_1	-4.07	-4.33	-4.33	-4.34	-4.34	-4.40
X_4	-3.75	-3.78	-3.79	-3.80	-3.80	-3.80
X_3	-3.18	-3.19	-3.20	-3.30	-3.29	-3.29
M_4	-6.36	-6.52	-6.54	-6.55	-6.54	-6.54
M_5	-5.03	-5.05	-5.07	-5.07	-5.07	-5.08
M_1	-3.77	-4.01	-4.01	-4.02	-4.02	-4.14
M_3	-2.81	-2.96	-2.97	-2.98	-2.98	-2.98
M_5	1.99	1.96	1.97	1.99	1.98	1.94
E_F	-3.75	-3.91	-3.92	-3.93	-3.93	-3.93

sian orbitals, permitting solutions to the Poisson equation to be obtained analytically. However, rapidly oscillatory behavior combined with extremely localized numerical errors found in ρ_{cry} at each nuclear site make the convergence of the expansion of $\delta\rho$ in symmetrized plane waves and/or Gaussian orbitals very slow. Since the net charge (volume integral of these localized numerical errors) is extremely small, their overall effect on the energies or wave functions are probably negligible. The simplicity of the discrete variational method does not limit expansion of the potential to any particular analytical form. Thus it is more convenient to expand $\delta\rho$ in region I in Kubic harmonics and solve the radial part of the Poisson equations numerically, whereas the slowly varying

$\delta\rho$ in the interstitial region (III) can be expanded in a rapidly convergent symmetrized plane-wave series. Generalization of this approach to the treatment of a full potential beyond the superposition of the overlapping spherical charge-density model is under development, and will be reported later.

In Sec. III we present results for one-, three-, and five-layer Ni (001) slabs; the integration parameters, SC charge configuration, and the degree of SC(Δ) are tabulated in Table I. The convergence in the energies and wave functions correspond closely to those given in column E of Tables III and IV of Appendix B. Note that the atomic configurations listed pertain only to the SC atomic charge density generated from numerical solution

TABLE IV. Comparison of the degree of self-consistency Δ (cf. Eq. 1) and the Mulliken charge analysis of the wave functions for the same sets of Diophantine points and approximations as defined in Table I.

Core	A Full	B Full	C Full	D Frozen	E Frozen	F Frozen
N_I	300	750	1000	1000	750	300
N_{III}	600	1500	2500	2500	1500	600
Δ	2.619	0.840	0.555	0.250	0.262	0.321
Mull 3d	8.54	8.60	8.60	8.62	8.62	8.62
4p	0.98	0.97	0.96	0.93	0.95	0.96
4p	0.44	0.41	0.42	0.45	0.43	0.42

of the same Hamiltonian for a free atom with the external potential well (in a.u.),

$$V(r) = \begin{cases} -1, & r < 7 \\ \frac{1}{28}r - 1.25, & 7 \leq r \leq 35, \end{cases} \quad (2)$$

added to avoid the possible formation of linear dependence in the virtual states of the LCAO Bloch basis. Because of the extensive overlapping of the free-electron-like $4s$-$4p$ states, the atomic configuration shown in Table I does not reflect the charge transfer between different layers. Note also that the SC potential for the one-, three-, and five-layer Ni (001) slabs had a least-mean-square error between the input superposition and the true crystal charge density of less than 1.87%, 0.83%, and 0.72% of their valence electrons per unit cell, respectively.

III. RESULTS

A. Energy-band structure

The self-consistent energy bands of the five-layer Ni (001) film are presented in Fig. 2 along the high-symmetry directions in the two-dimensional BZ. In order to clarify the band structure, states of $\overline{\Delta}_2 - \overline{Y}_2 - \overline{\Sigma}_2$ symmetry are displayed above those of $\overline{\Delta}_1 - \overline{Y}_1 - \overline{\Sigma}_1$ symmetry. In addition, the wave functions have either even or odd parity with respect to reflection about the central plane. For a given two-dimensional symmetry, only bands of opposite parity are allowed to cross one another. The general trend in the energy bands (opening of gaps, bandwidths, etc.) agrees quite well with the parametrized LCAO calculation of Dempsey and Kleinman[8] for a 35-layer spin-polarized Ni (001) film. There, extremely localized surface states of majority spin (X_4) and doubly degenerate (X_5) states were found to be essential[8] for accounting for the reversal of the photoelectron spin polarization observed[17] 0.1 eV above the threshold. The limitation of a film thickness of five layers does not permit a thorough study of the surface states. However, the existence and symmetry of the surface states was found by Caruthers and Kleinman[10] to depend crucially on details of the potential. The simple SC procedure described in this paper appears to be an ideal way to investigate the surface states in a thicker film. The variational freedom of the LCAO basis set can be improved by adding additional virtual atomic states or symmetrized plane waves in order to describe the surface states that may peak more than a half layer outside the surface plane. The surface states of a Ni (001) film are investigated in a future publication, where we extend our calculation to treat a thicker film.

    Surface and finite thickness effects can be better
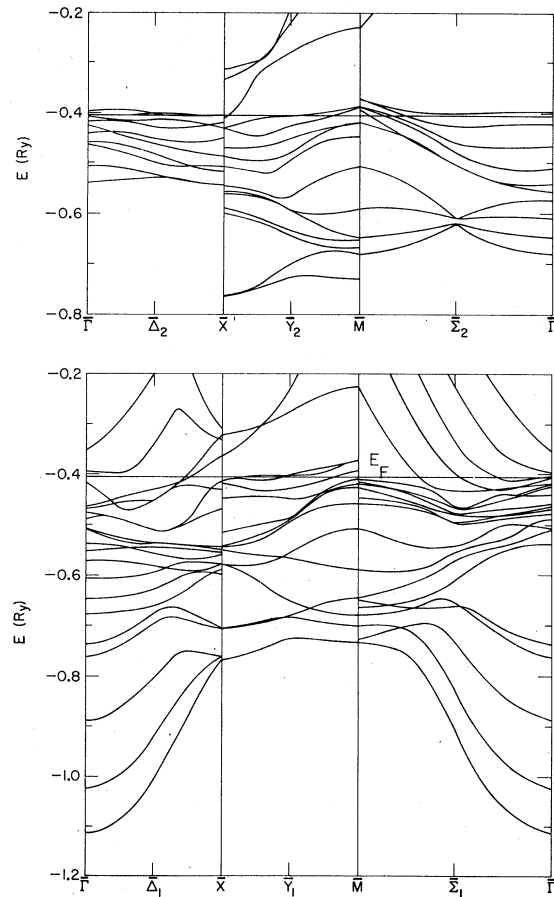
FIG. 2. Energy-band structure of the five-layer Ni (110) film plotted along the high-symmetry directions in the two-dimensional BZ. The upper panel shows the states that have $\overline{\Delta}_2 - \overline{Y}_2 - \overline{\Sigma}_2$ symmetry and the lower panel the states of $\overline{\Delta}_1 - \overline{Y}_1 - \overline{\Sigma}_1$ symmetry.

understood by comparing the projected surface band structure with that of the bulk system as proposed by Caruthers et al.[33] Note that the two-dimensional unit cell is rotated 45° in the xy plane away from the edge of the cube with length $a/\sqrt{2}$. To construct the projected band structure, we show in Fig. 3(a) the projection of a three-dimensional fcc unit cell defined by direct-lattice vectors $a(\frac{1}{2}, \frac{1}{2}, 0)$, $a(\frac{1}{2}, -\frac{1}{2}, 0)$, and $a(0, 0, 1)$ that is commensurate with that of the two-dimensional surface unit cell. The corresponding projection of the three-dimensional BZ defined by reciprocal-lattice vectors $(\vec{K}) = (2\pi/a)(1, 1, 0)$, $(2\pi/a)(1, -1, 0)$, and $(2\pi/a)(0, 0, 1)$ are shown in Fig. 3. Symmetry points in the two-dimensional BZ are denoted by an overbar. Now in the limit of infinite film thickness the energies at a point $\vec{k}$ in the two-dimensional BZ span all the points at $(\vec{k}, k_z) + \vec{K}$ in the three-dimensional BZ, where $-\pi/a \leq k_z \leq \pi/a$. The two-dimensional energy levels at the $\overline{\Gamma}$, $\overline{M}$, and $\overline{X}$
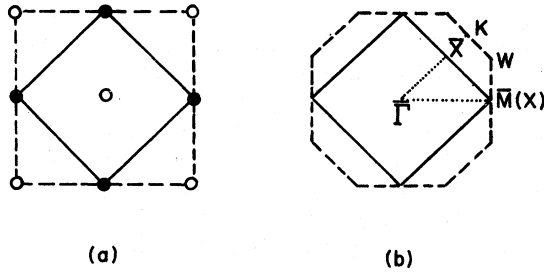
FIG. 3. (a) Projection of a three-dimensional fcc unit cell defined by the direct lattice vectors $a(\frac{1}{2},\frac{1}{2},0)$, $a(\frac{1}{2},-\frac{1}{2},0)$ and $a(0,0,1)$. The solid lines represent the base of the commensurate unit cell. (b) The corresponding projection of the three-dimensional BZ defined by the reciprocal-lattice vectors $(\vec{K}=(2\pi/a)(1,1,0)$, $(2\pi/a)(1,-1,0)$, and $(2\pi/a)(0,0,1)$.

points are used to reconstruct the three-dimensional energy bands in Fig. 4 along Δ, Z, and L to $(\pi/a)(\frac{1}{2},\frac{1}{2},0)$ directions, respectively. The unpublished band-structure results of Wang and Callaway[34] for paramagnetic bulk Ni are also included for comparison (solid lines, but with the origin of the bulk energy bands shifted in order to align the Fermi energies). Note that states of $\Delta_2(x^2-y^2)$, $\Delta_2'(xy)$ symmetry agree very well with that of the bulk results, while states of $\Delta_5(xz,yz)$ symmetry, whose lobes at the surface atoms point toward the missing nearest-neighbor atom sites, deviate slightly more. A rather large downward shift of 0.05 Ry was found in the Δ_1 states of predominantly sp character relative to the d-band complex.

The fact that the Γ_1 state projected from a five-layer film lies below that of the bulk result is
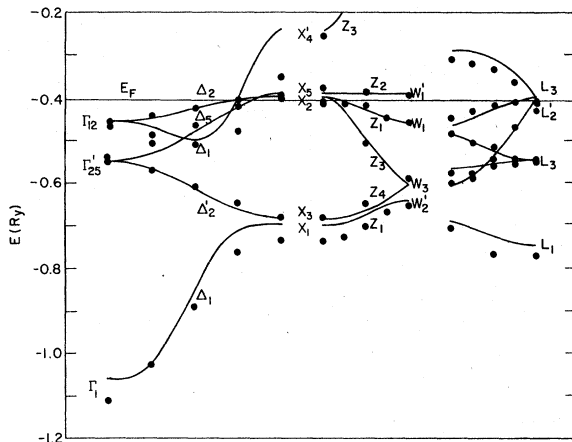
rather surprising, since the bandwidth of both the sp and d bands are expected to be narrower in a thin film. The initially assumed non-SC potential yields a value for $E_F-\Gamma_1$ that is 0.08 Ry larger than that for the SC results. However, when we compare the width of the projected sp states along the Δ direction, we find indeed a narrowing of 0.05 Ry, i.e., in a thin film the sp bands are driven down in energy relative to the d bands. It is interesting to note that a lowering of the Γ_1 level by 0.01 Ry was also reported[33] in a non-SC calculation for a 13-layer Al (001) film when compared with the result of an equivalent bulk calculation for Al. The magnitude was found to be dependent on the surface-to-volume ratio of the film [e.g., it was reduced to 0.005 Ry in a 39-layer Al (001) film]. In a supplemented orthogonalized-plane-wave (OPW) calculation for a 13-layer Fe (001) film,[10] it was found that the width of the sp band and the position of the bottom Γ_1 level relative to E_F were substantially increased when the $X\alpha$ exchange potential was reduced by varying α from 1 to $\frac{2}{3}$. Similarly, the value of $\Gamma_{25}'-\Gamma_1$ was found to increase with decreasing α in a SC calculation for bulk Cu.[35] For these reasons, we tentatively associate the lowering of the Γ_1 state of a five-layer film in Fig. 4 with the reduction of the superposition charge density, and hence of the exchange potential from the bulk values near the surface region.

The convergence with respect to the film thickness is examined in Fig. 5, where the projection of the $\bar{\Gamma}$ level onto the Δ direction for the one-, three-, and five-layer films are compared. Note

FIG. 4. Reconstruction of the three-dimensional band structure along the Δ, Z, and L to $(\pi/a)(\frac{1}{2},\frac{1}{2},0)$ directions using the two-dimensional energy eigenvalues at the $\bar{\Gamma}$, $\bar{M}$, and $\bar{X}$ points, respectively. The bulk band structure for paramagnetic Ni (solid lines) of Wang and Callaway are shown for comparison.
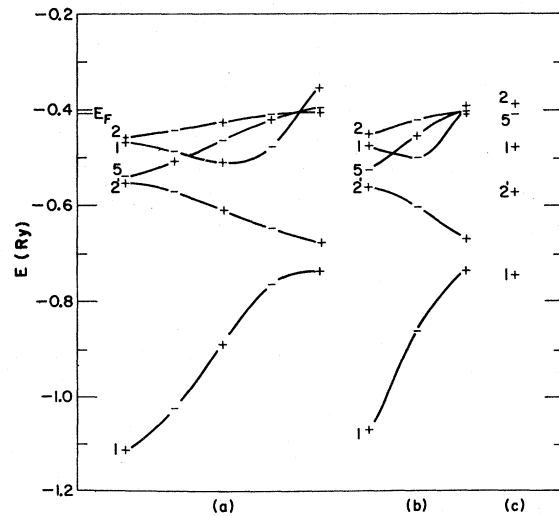
FIG. 5. Projection of the $\bar{\Gamma}$ level onto the Δ direction for the (a) five-, (b) three-, and (c) one-layer films. The (+) and the (−) symbols are used to denote even or odd parity with respect to reflection about the central plane.

that whereas the d-band complex can be described rather well by a three-layer film compared with the five-layer result, the plane-wave states (Δ_1) in the three-layer film are narrower. As the film thickness increases, the splitting of the levels, which for three-dimensional symmetry points are degenerate, gradually disappears. In the extreme case of a monolayer, the widths of both the d band and the sp states are much narrower and the resulting center of the d bands is found to lie relatively high in energy.

B. Density of states

The density of states (DOS) and the projected local DOS are compared in Fig. 6 for the one-,

three-, and five-layer Ni (001) films. The two-dimensional DOS is seen to have more structure than does the three-dimensional DOS because the continuous spectrum along the z direction in the case of the bulk is replaced by discrete energy levels in the thin-film case. From the computational side, we also expect more numerical instability in the case of a film, since the convergence of the k integration is degraded by the increasing number of accidental degeneracies allowed in the two-dimensional symmetry plane. Originally, the DOS was calculated from a sampling of 15 $\bar{k}$ points in $\frac{1}{8}$ of the irreducible zone using the triangle scheme described in Appendix A. These results were then smoothed by a Gaussian broadening function of 0.1 eV full width at
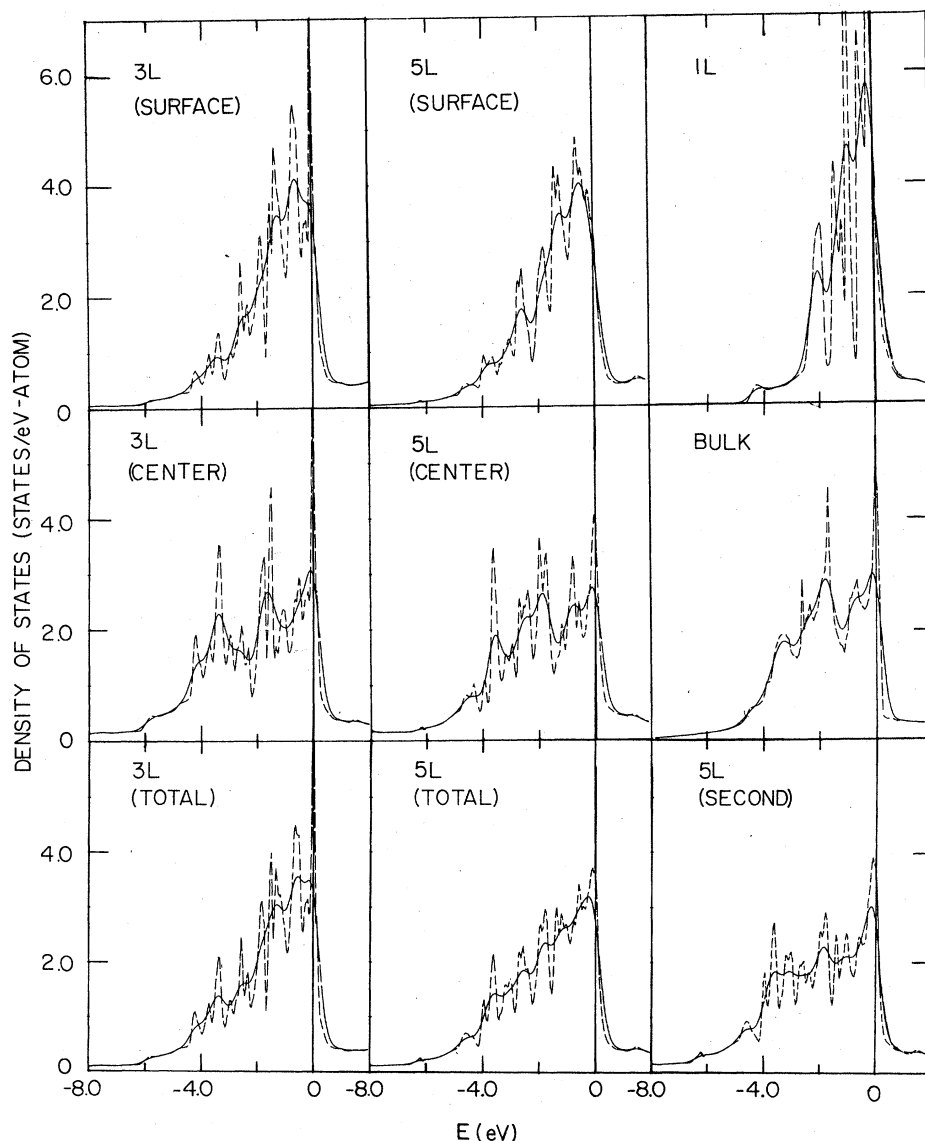
FIG. 6. Density of states and projected local density of states for the one-, three-, and five-layer Ni (001) films in units of electron states/atom-eV. The dashed curves are the raw curves smoothed by a Gaussian broadening function of 0.1 eV FWHM; the solid curves are the result of a similar broadening of 0.5 eV. The bulk DOS for paramagnetic Ni of Wang and Callaway (Ref. 36) is shown in the right-hand center panel.

half maximum (FWHM) (dashed lines in Fig. 6) to permit all detailed structures to be preserved when comparing results of different theoretical models. [Note that this smoothing procedure was not necessary in the DOS of bulk Ni[34] (shown as dashed lines in the second box on the right), as this was calculated using 505 points in $\frac{1}{48}$ of the BZ.] The DOS shown as solid lines in Fig. 6 were smoothed by a Gaussian fold of 0.5 eV FWHM in order to compare with the different experimental results. One sees that there are distinctive differences between the surface-plane (SP) and center-plane (CP) projected DOS in either the three-layer (left-hand column) or five-layer (center column) results. The CP DOS consists of three major peaks located at approximately 0.3, 1.9, and 3.6 eV below E_F. Each peak in the five-layer film has an additional shoulder that would be smoothed if a larger FWHM Gaussian fold were used. The way the three- and five-layer CP DOS converge toward the bulk DOS is very encouraging, in that it provides some direct evidence for the adequacy of describing the surface properties using thin films of only five atomic layers thick.

The severe narrowing of the d bands and the accompanying upward shift of its center of gravity that we reported in our earlier study of a Cu monolayer[31] was also found in the case of a Ni monolayer (see the top panel in the right-hand column of Fig. 6). These effects are a direct consequence of the reduction in the number of nearest-neighbor atoms at the surfaces. Similar, but smaller, changes are observed in our SP DOS for three- or five-layer films. In contrast to the CP DOS, the SP DOS exhibits a major peak at about -0.6 eV, with three weak shoulders on its rapidly decreasing side of the DOS at lower energies. These differences between the SP and CP DOS, and in the five-layer case also with the second plane DOS (bottom panel in the right-hand column), may be important in interpreting results obtained with surface-sensitive spectroscopies (if one has escape depth information to include in the analysis[36-38]). The five-layer DOS (bottom panel in the center column) still differs substantially from the bulk DOS since $\frac{2}{5}$ of the contribution arises from the SP DOS. Thus it is very important to properly separate and weight the contribution from the SP DOS in order to understand the role of the surfaces in a thin-film model.

One reason that our projected DOS differs from the recent self-consistent LCGO results for a three-layer Ni (001) film by Smith et $al.$[14] is the different means employed in carrying out the projection. Whereas the results shown in Fig. 6 were weighted at each k point by the Mulliken charge and population analysis of the wave functions, the re-

sults of Smith et $al.$ were weighted by the sum of the square of the coefficients of the basis functions in that plane.[13,14] However, since the LCGO basis functions are not orthogonal, the contribution from the off-diagonal elements of the overlap matrices have been neglected, making the sum of their calculated projected DOS not equal their calculated total DOS. This argument does not account, however, for the discrepancy seen in comparing the two total DOS's. We believe that our total DOS is the correct one, since our center-plane DOS has been found to converge to the bulk DOS.

C. Fermi energy

The Fermi energy (E_F) for the SC one-, three-, and five-layer film are compared in Table II. Note that the E_F for the five-layer slab converged from its initial value of -9.14 eV (superposition of neutral atom $3d^{8.5}4s^14p^{0.5}$ potentials) to -5.52 eV, which is in reasonable agreement with the measured work function of 5.15–5.27 eV.[17,39,40] In a SC calculation for a bulk system, the origin of the energy bands has no effect on the electronic wave functions because the solution of Poisson's equation is not affected by a rigid shift in the potential. However, a reasonable value of E_F in a SC calculation for surfaces ensures that the potential diminishes as it approaches the vacuum region with a proper surface dipole moment. The present theory does not include many-body effects, such as the work done against the image force in removing an electron from the metal.[41] The sensitivity of the E_F with respect to the degree of SC(Δ) is not sufficient for us to make a quantitative estimate of the possible many-body effects for the following reasons: Since the charge density ρ decays much faster than the $\rho^{1/3}$ exchange potential in the selvage region, the charge-density self-consistency employed here does not monitor the tail of the potential beyond the range of ρ. Furthermore, the least-squares fitting procedure in our SC process emphasizes the high-density limit (which affects details of the energy bands) more than the low-density region (which tends to rigidly shift the potential). Other than a possible error of 7% in the estimate of E_F, the uncertainty in the long tail of the potential has very little effect on the ground-state properties presented in other sections of this paper.

D. Charge density

Finally, we present in Fig. 7 the SC valence electronic charge-density map of a five-layer Ni (001) film on the (110) plane with the surface normal along the vertical section. It is interesting to note the way the charge density gradually
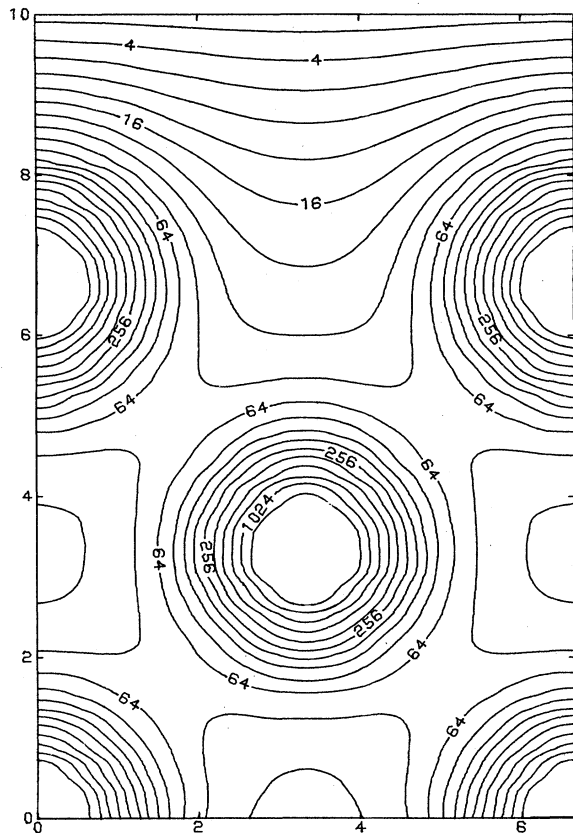
FIG. 7. Self-consistent conduction-electron charge-density map in units of 0.001 eV shown in the (110) plane as obtained from five-layer Ni (001) film calculation. Each contour line differs by a factor of $\sqrt{2}$.

smooths out parallel to the surface as one enters into the vacuum region. Figure 7 agrees with the result of Gay et al.[13] for a three-layer Cu (001) film in that the charge density at one layer below the surface already appears to be bulklike. Around each atom there is a fairly large region where the charge density is spherically symmetric. Therefore, the commonly used muffin-tin approximation, which assumes spherical symmetry around each atom, z dependence outside the surface plane, and the constant in the interstitial region, is quite adequate except in the interstitial region on the surface plane, where the charge density varies more rapidly due to the open surface structure.

IV. DISCUSSION OF SELF CONSISTENCY

The most important effects of SC in a surface calculation, the amount of charge transfer that occurs near the surface, can be determined by a direct numerical integration of the charge density over the nearest volume of each atomic site. Results obtained by integrating the SC ρ_{cry} and ρ_{sup}

for the five-layer slab are compared in Table II with those calculated from the initially assumed non-SC potential. Corresponding results evaluated according to the Mulliken analysis are also included for comparison. Note that the non-SC wave functions based on the superposition of the neutral $3d^{8.5}4s^{1}4p^{0.5}$ atomic potential yield a *deficit* of 1.2 e/at. on the surface plane in spite of the fact that the initial superposition charge density used as input to the starting potential is practically neutral on the surfaces. This is not entirely surprising, since the potential on the surface diminishes gradually as it approaches the vacuum region; if the initially assumed potential rises too fast in the selvage region, then electrons will be pushed into the center. Upon achieving SC, there is an *excess* of 0.03 e/at. on the surface layer. This small amount of surface charge is in agreement with the result of a jellium calculation,[42] which predicts that the Friedel oscillations are suppressed in a high-density electron gas.

In a recent supplemented OPW calculation for a 13-layer paramagnetic Fe (001) thin film, using a non-SC warped muffin-tin potential [superposition of $3d^{7}4s^{1}$ atomic charge densities and Slater exchange ($\alpha = 1$) approximation], Caruthers et al.[9] found a surplus of 1.5 e/at. on the surface plane. This is much larger than either the result of their parametrized LCAO calculation for ferromagnetic Fe (Ref. 6) (a deficit of 0.52 e/at.) or the paramagnetic Fe results of Desjonqueres and Cyrot-Lackmann[7] (a surplus of similar magnitude). Caruthers et al. then concluded that "all LCAO calculations yield too few surface electrons simply because the LCAO basis cannot account for the electronic charge in the selvage region." We disagree with this conclusion for several reasons: First of all, Table II demonstrates the sensitivity of the surface charge transfer to the choice of the right SC potential. Second, the large SP Friedel peak shown in Fig. 7 of Ref. 9 is localized inside the muffin-tin sphere; only a small contribution comes from the selvage region. Finally, the surface electrons tend to relax from the bulk system back to more atomiclike behavior due to the reduction in the number of nearest-neighbor atoms. The major modification in the charge density arises from the loss of reflection symmetry about the SP and the radial redistribution that accompanies the Friedel-type oscillations. In this respect, an LCAO basis (including $4p$ states) should have no more difficulty than a warped muffin-tin potential that assumes spherical symmetry about each surface atom inside the muffin-tin sphere. We believe that the discrepancy in the different non-SC theoretical calculations simply reflects the difference in their potentials or the different choice of surface

parameters. A unique solution can be derived if the potentials are evaluated self-consistently.

ACKNOWLEDGMENTS

APPENDIX A: ANALYTIC-TRIANGLE-LINEAR-ENERGY METHOD

In this section we describe the analytic-triangular-linear-energy method, as generalized from the linear-analytical-tetrahedron method[22-24] to integrate over the two-dimensional BZ. The orbital density of states is defined as

$$G_\mu(E) \frac{2A}{(2\pi)^2} \sum_i \int M_{i\mu}(\overline{k})\, \delta[E - E_i(\overline{k})]\, d^2\overline{k} ,$$

(A1)

where A is the area of the unit cell. A factor of 2 has been included to account for spin degeneracy in Eq. (A1). The total density of states $G(E)$ can simply be obtained by setting

$$M_{i\mu}(\overline{k}) = 1 .$$

(A2)

In order to calculate the local density of states projected onto orbital μ according to the Mulliken charge and population analysis,[30] we define

$$M_{i\mu}(\overline{k}) = \sum_\nu c_{i\mu}^*(\overline{k})\, c_{i\nu}(\overline{k})\, S_{\mu\nu}(\overline{k}) ,$$

(A3)

where $c_{i\mu}(\overline{k})$ and $S_{\mu\nu}(\overline{k})$ are the eigenvectors and overlap matrices, respectively. For a given band index (i), the summation includes all basis (ν). Equation (A1) can also be expressed as an integral over a line of constant energy E in the BZ

$$G_\mu(E) = \frac{2A}{(2\pi)^2} \sum_i \int M_{i\mu}(\overline{k}) \left(\frac{dl_k}{|\nabla E_i(\overline{k})|} \right)_{E_i(\overline{k})=E} .$$

(A4)

The BZ is first divided into triangles, with corners of a given triangle labeled $\overline{k}_1 \overline{k}_2 \overline{k}_3$ such that $E_1 \leq E_2 \leq E_3$, and use the notation $E(\overline{k}_s) = E_s$ and $M_\mu(\overline{k}_s) = M_s^\mu$. For illustration, we consider only a single band so that the band index is dropped. The contribution from each triangle can be integrated analytically if we assume that $E(\overline{k})$ and $M^\mu(\overline{k})$ are linear inside the triangle. We find that

$$g_\mu(E) = \frac{2A}{(2\pi)^2} \left(2B \frac{(E-E_1)}{(E_2-E_1)(E_3-E_1)} \right) \left(M_1^\mu + \frac{E-E_1}{2(E_2-E_1)}(M_2^\mu - M_1^\mu) + \frac{E-E_1}{2(E_3-E_1)}(M_3^\mu - M_1^\mu) \right) \text{ if } E_1 \leq E \leq E_2 ,$$

(A5)

or

$$g_\mu(E) = \frac{2A}{(2\pi)^2} \left(2B \frac{E_3-E}{(E_3-E_1)(E_3-E_2)} \right) \left(\frac{M_1^\mu + M_2^\mu}{2} + \frac{E-E_1}{2(E_3-E_1)}(M_3^\mu - M_1^\mu) + \frac{E-E_2}{2(E_3-E_2)}(M_3^\mu - M_2^\mu) \right) \text{ if } E_2 \leq E \leq E_3 ,$$

(A6)

where B is the area of the triangle. The contribution from each triangle to the integrand density of states $n(E)$, defined as

$$n(E) = \int_{-\infty}^{E} g(E')\, dE' ,$$

(A7)

can be obtained directly from Eq. (A5) or (A6).

The Fermi energy E_F is determined by setting $N(E_F)$ equal to the total number of electrons in the unit cell. It is possible to determine E_F efficiently without actually calculating $G(E)$. The energy range is first divided into a few intervals where $N(E)$ is evaluated. The interval that contains E_F is then subdivided to obtain a new energy range over which $N(E)$ is evaluated. The search is continued until the desired accuracy is obtained in the determination of E_F. The only approximation is the assumption that the energy is assumed to be linear inside each triangle; of course, as the number of triangles increases (and the size of each decreases), this approximation gets better and better.

More general integrals involving a step function occupation at the Fermi energy

$$F = \int f(\bar{k}) \, \Theta \, [E_F - E(\bar{k})] \, d^2\bar{k} \tag{A8}$$

can also be obtained analytically if we assume linearity of the integral $f(\bar{k})$ inside each triangle. If the triangle is completely occupied, then

$$F = \tfrac{1}{3}B \, [f(\bar{k}_1) + f(\bar{k}_2) + f(\bar{k}_3)] \, . \tag{A9}$$

For a partially filled triangle, the integral can be evaluated by (i) using the smaller occupied triangle if $E_1 \leqslant E_F \leqslant E_2$:

$$F = \frac{B'}{3} \left[\left(1 + \frac{E_2 - E}{E_2 - E_1} + \frac{E_3 - E}{E_3 - E_1} \right) f(\bar{k}_1) \right.$$
$$\left. + \frac{E - E_1}{E_2 - E_1} f(\bar{k}_2) + \frac{E - E_1}{E_3 - E_1} f(\bar{k}_3) \right] , \tag{A10}$$

where B' is the area of the occupied triangle, or (ii) by subtracting the contribution of the unoccupied triangle if $E_2 \leqslant E_F \leqslant E_3$:

$$F = \frac{B}{3} [f(\bar{k}_1) + f(\bar{k}_2) + f(\bar{k}_3)]$$
$$- \frac{B''}{3} \left[\frac{E_3 - E}{E_3 - E_1} f(\bar{k}_1) + \frac{E_3 - E}{E_3 - E_2} f(\bar{k}_2) \right.$$
$$\left. + \left(1 + \frac{E - E_1}{E_3 - E_1} + \frac{E - E_2}{E_3 - E_2} \right) f(\bar{k}_3) \right] . \tag{A11}$$

where B'' is the area of the unoccupied portion of the triangle.

APPENDIX B: NUMERICAL CONVERGENCE TESTS ON Ni (001) MONOLAYER

The energy bands of a monolayer of Ni (001) film calculated at high-symmetry points for a superposition potential (atomic configuration $3d^9 4s^1$), using different sets of Diophantine points in region I (N_I) and III (N_{III}) with $R = 2.2$ a.u. and $L = 8.324\,25$ a.u., and either frozen- or full-core basis sets are compared in Table III. Note that in column F the frozen-core results are converged to within 0.09 eV for $N_I = 300$, $N_{III} = 600$, while the corresponding full-core basis results (column A) still differ by as much as 0.26 eV. However, both types of basis sets are converged to within 0.02 eV when $N_I = 750$ and $N_{III} = 1500$ points are used (columns C and D). From the same table, we can also see that by freezing the core basis, we have made overall errors of less than 0.02 eV in the d-band complex and 0.1 eV in the relative position of the s, p, and d levels.

In Table IV we compare the convergence of the wave functions by examining Δ and the Mulliken charge analysis of the wave functions for the same sets of Diophantine points given in Table III. Note that the Mulliken charge analysis for the frozen-core basis converged to slightly different results than those obtained with the full-core basis due to the changes in the orthogonalized LCAO Bloch functions. For the frozen-core basis, $\Delta(N_I = 750, N_{III} = 1500)$ has converged to within 5% when compared with that of $\Delta(N_I = 1000, N_{III} = 2500)$, while the corresponding full-core basis value of Δ still differs by 51%. The remaining small unsystematic numerical errors in $\rho_{cry}(r)$ in r space cannot be fitted within the limited superposition model; they are effectively averaged in the least-mean-square fitting process during each SC cycle. (We found in several cases that the difference found for Δ between the initial and SC potential calculations remains approximately the same even though Δ itself can be further reduced by increasing N_I and/ or N_{III}.) Therefore Δ should be viewed in the superposition model as an upper bound to the difference $\delta\rho$ between ρ_{sup} and the true ρ_{cry}.

[1] B. R. Cooper, Phys. Rev. Lett. 30, 1316 (1973); Phys. Rev. B 16, 5595 (1977).

[2] R. V. Kasowski, Phys. Rev. Lett. 33, 83 (1974); 33, 1147 (1974); 37, 219 (1976); Solid State Commun. 17, 179 (1975).

[3] N. Kar and P. Soven, Phys. Rev. B 11, 3761 (1975).

[4] S. J. Gurman, J. Phys. F 5, L194 (1975).

[5] K. S. Sohn, D. G. Dempsey, L. Kleinman, and E. Caruthers, Phys. Rev. B 13, 1515 (1976); 14, 3185 (1976); 14, 3193 (1976); D. G. Dempsey and L. Kleinman, ibid. 16, 5356 (1977).

[6] D. G. Dempsey, L. Kleinman, and E. Caruthers, Phys. Rev. B 12, 2932 (1975); 13, 1489 (1976); 14, 279 (1976); J. Phys. F 7, 113 (1977).

[7] M. C. Des jonqueres and F. Cyrot-Lackman, J. Phys. F 5, 1368 (1975).

[8] D. G. Dempsey and L. Kleinman, Phys. Rev. Lett. 39, 1297 (1977).

[9] E. Caruthers, D. G. Dempsey, and L. Kleinman, Phys. Rev. B 14, 288 (1976).

[10] E. Caruthers and L. Kleinman, Phys. Rev. Lett. 35, 738 (1975).

[11] S. G. Louie, K. M. Ho, J. R. Chelikowsky, and M. L. Cohen, Phys. Rev. Lett. 37, 1289 (1976); Phys. Rev. B 15, 5627 (1977).

[12] K. M. Ho, S. G. Louie, J. R. Chelikowsky, and M. L. Cohen, Phys. Rev. B 15, 1755 (1977).

[13] J. G. Gay, J. R. Smith, and F. J. Arlinghaus, Phys. Rev. Lett. 38, 561 (1977).

[14] J. R. Smith, F. J. Arlinghaus, and J. G. Gay, Inst. Phys. Conf. Ser. 39, 303 (1978).

[15] C. S. Wang and J. Callaway, Phys. Rev. B 15, 298 (1977); J. Callaway and C. S. Wang, ibid. 16, 2095 (1977); D. G. Laurent, C. S. Wang, and J. Callaway, ibid. 17, 455 (1978).

[16] J. F. Janak and A. R. Williams, Phys. Rev. B 14, 4199 (1976); V. L. Moruzzi, A. R. Williams, and J. F. Janak, ibid. 15, 2854 (1977); J. F. Janak, ibid. 16, 255 (1977).

[17]W. Eib and S. F. Alvardo, Phys. Rev. Lett. 37, 444 (1976).

[18]Since the center plane of the slab is a reflection plane, the Hamiltonian was block diagonalized to two ~500 ×500 matrices using the technique of symmetrized plane waves.

[19]In Ref. 15, the majority-spin L_2' state of ferromagnetic bulk Ni was found to sometimes oscillate about the Fermi energy in the iterative procedure toward SC. It was found very helpful to use an analytic linear energy tetrahedron method to sample the charge density accurately according to the cutoff of the Fermi energy.

[20]D. E. Ellis and G. S. Painter, Phys. Rev. B 2, 2887 (1970).

[21]A. Zunger and A. J. Freeman, Phys. Rev. B 15, 4716 (1977).

[22]O. Jepsen and O. K. Andersen, Solid State Commun. 9, 1763 (1971).

[23]G. Lehman and M. Taut, Phys. Status Solidi 54, 469 (1972).

[24]C. S. Wang and J. Callaway, Comp. Phys. Commun. 14, 327 (1978); J. Rath and A. J. Freeman, Phys. Rev. B 11, 2109 (1975).

[25]W. Kohn and L. J. Sham, Phys. Rev. A 140, 1133 (1965).

[26]P. P. Ewald, Ann. Phys. (Leipz.) 64, 753 (1971).

[27]W. Y. Ching and C. C. Lin, Phys. Rev. B 12, 5536 (1975).

[28]F. Herman and S. Skillman, *Atomic Structure Calcula-tion* (Prentice-Hall, Englewood Cliffs, 1963).

[29]C. B. Haselgrove, Math. Compt. 15, 373 (1951).

[30]R. S. Mulliken, J. Chem. Phys. 23, 1833 (1955).

[31]C. S. Wang and A. J. Freeman, Phys. Rev. B 18, 1714 (1978).

[32]C. S. Wang and A. J. Freeman, Bull. Am. Phys. 23, 361 (1978).

[33]E. Caruthers, L. Kleinman, and G. P. Alldredge, Phys. Rev. B 8, 4570 (1973).

[34]C. S. Wang and J. C. Callaway (unpublished results) [paramagnetic version of J. C. Callaway and C. S. Wang, Phys. Rev. B 7, 1096 (1973)].

[35]J. F. Janak, A. R. Williams, and V. L. Moruzzi, Phys. Rev. B 6, 4367 (1972).

[36]P. J. Feibelman and D. E. Eastman, Phys. Rev. B 10, 4932 (1974).

[37]R. Haydock, V. Heine, M. J. Kelly, and J. B. Pendry, Phys. Rev. Lett. 29, 868 (1972).

[38]M. Mehta and C. S. Fadley, Phys. Rev. Lett. 39, 1569 (1977).

[39]D. E. Eastman, Phys. Rev. B 2, 1 (1970).

[40]Y. Fukuda, W. T. Elam, and R. L. Park, Phys. Rev. B 16, 3322 (1977).

[41]N. D. Lang and W. Kohn, Phys. Rev. B 3, 1215 (1971); R. Monnier, J. P. Perdew, D. C. Langreth, and J. W. Wilkins, *ibid.* 18, 656 (1978).

[42]N. D. Lang and W. Kohn, Phys. Rev. B 1, 4555 (1970).